RSC Advances

ROYAL SOCIETY OF CHEMISTRY

www.rsc.org/advances

Throwing light on hydroxyquinoline-based ruthenium sensitizers with long-lived charge carrier boosts photocatalytic H$_2$ evolution

Indranil Mondal,[a,b] Amritanjali Tiwari,[a,b] Rajib Ghosh,[c] Ujjwal Pal*[a,b]

[a.] *Central Mechanical Engineering Research Institute, M. G. Avenue, Durgapur-713209, WB, India.*

[b.] *Network of Institutes for Solar Energy (CSIR-NISE) and Academy of Scientific and Innovative Research (AcSIR)*

[c.] *Radiation & Photochemistry Division Bhabha Atomic Research centre, Mumbai-400085, India*

Abstract

Three new hydroxyquinoline coordinated ruthenium (II) sensitizers bearing polypyridyl derivatives anchor (**R1, R2** and **R3**) were synthesized that tethers to visible light sensitization over Pt-TiO$_2$ system for hydrogen production. The highest hydrogen production yield was obtained with 225.2 µmol and turnover number (TON) 1734 (for 6 h) over **R1**/Pt-TiO$_2$. The photoactivity of the as-prepared sensitizers was found to be predominantly influenced by longer lifetime of metal-to-ligand-charge transfer (MLCT) states with suitable redox properties of transient Ru (II) species in the heteroleptic complexes. The measurement of binding kinetics revealed a comprehensive understanding between the adsorption behaviour of dyes on to TiO$_2$ surface and ligand influence on the hydrogen evolution activity. The dependence of the hydrogen generation rate was systematically screened at different dye concentrations (0.05-1.0 µmol/10 mg TiO$_2$) and the results were correlated with their pertinent adsorption properties. The operational parameters like, pH of the medium and noble metal loading were taken into account for optimal photocatalytic performance.

Introduction

Visible light harvesting through semiconductor photocatalysis is a key technology for solar chemical conversion process. Although titania nanoparticles are popular as a base material of photocatalysis, the lack of visible light activity needs to be overcome, as TiO$_2$ with large band gap (~3.2 eV) can only harvest the UV light which covers only 5% of sunlight. Solar water splitting under UV irradiation using TiO$_2$ and a Pt black system was first reported by Honda and Fujishima.[1] Later, extensive research efforts have been made to modify the TiO$_2$ surfaces with a visible light active component, in order to achieve high solar energy conversion efficiency. Dye sensitization on semiconductor surface came with good strategic potential since the discovery of dye sensitized solar cell by Grätzel and co-workers in 1991.[2] Over the course of time, there has been some remarkable progress in the design and development of dyes,[3] yet there should definitely be more extensive studies and clear understanding about sensitizers for fabricating more active systems. Implementation of different ligand system to acquire desirable photophysical properties is under intensive focus area for ruthenium(II) complexes in the application of DSSC,[4a,b] even phthalocyanines could be a potential alternative for this purpose.[4c] Ruthenium heteroleptic complexes to date has been extensively pursued as the photosensitizer due to long-lived ligand-centered excited-state lifetimes and fine-tuned redox properties, to achieve optimal material characteristics.[5] Especially thiocyanate based ruthenium complexes are well known for showing longer wavelength-absorbing nature.[4a] Apart from optical and electrochemical features, many other properties like dye adsorption, aggregation, dissolution and regeneration are very crucial parameters for controlling the electron transfer during photocatalytic reaction.[6] In this regard, a marked progress has been appreciated, but still a clear understanding is needed to synthesize much efficient systems. As of now, Ru,[7] Pt,[8] Ni complexes,[9] metalloporphyrins[10] and phthalocyanines[11] have been

successfully employed as the inorganic sensitizers for visible-light induced hydrogen production from water. In particular, Peng and co-workers[12] have well established a dimeric ruthenium complex ($[Ru_2(bpy)_4(BL)(ClO_4)_2]$ where bpy= bipyridyl, BL= bridging ligand) without any conventional anchoring group, exhibited "antenna effect" in photocatalytic hydrogen production reaction, but dye adsorption properties and its influence on the electron injection needs more attention. It is also noteworthy that, easy synthesis method and incorporation of simple ligand system is also another challenge in terms of commercial implications. However, as far as we are aware, the application of Ru-complex bearing simple ligand system like hydroxyquinoline or its derivative has not been developed before for photocatalytic H_2 evolution from water.

Here in, we report the syntheses of three new heteroleptic ruthenium sensitizers (coded as **R1**, **R2** and **R3**, presented in Fig. 1) featuring a hydroxyquinoline (HQ) based ancillary ligand, which endowed highly efficient visible light induced photocatalytic hydrogen production over Pt-TiO$_2$ system. We found that these heteroleptic complexes containing bipyridyl ligands tethered with carboxylic acid and long chain aliphatic group exhibited interesting structural influence on visible-light sensitization and photoinduced proton reduction from water and sacrificial electron donor (SED) mixture. We have also emphasized the role of coordinating ligands in tuning of optical, electronic and surface binding kinetic properties of sensitizers. Density functional theory (DFT) calculations were carried out for **R1** to **R3** to understand their structural and electronic properties.

Experimental section

The sensitizers (**R1, R2** and **R3**) were synthesized using facile techniques, including hydrothermal method in order to achieve the better ligand solubility.[13] The details of synthetic procedure of sensitizers and photocatalysts, and characterization of dye are incorporated in ESI†.

Photocatalytic experiment

The photocatalytic hydrogen generation experiments were carried out in a 100 ml Pyrex glass reactor with a flat optical entry window and external cooling jacket. 20 ml of aqueous suspension containing 10 mg of photocatalysts and 10 vol% of SED was taken as the reaction mixture. The reactor was sealed with silicon septum and kept under ultrasonic treatment for 2 min to suspend the catalysts completely in the water/SED system. Before light irradiation, dissolved oxygen was removed by 20 min evacuation followed by bubbling of argon gas for 30 min. As an external light source, 450 W xenon arc lamp (set at 400 W) used for the illumination on the suspended photocatalysts under constant stirring condition. A 420 nm cut off filter was used to illuminate only visible light. The distance between the lamp and the photoreactor containing reaction solution was fixed at 8 inches. The resulting evolved gases were analyzed by Perkin Elmer Clarus 580 GC equipped with 5Å molecular sieve column, a thermal conductivity detector (TCD) and Argon as the carrier gas. Intensity of the light was measured to be 2 sun.

Nanosecond flash photolysis experiment

Nanosecond flash photolysis studies were carried out by a Laser Kinetic Spectrometer from Edinburgh Instruments, UK, (model: LP920). The samples were taken in a 1 cm ×1 cm cuvette and were excited with a 7 ns pulsed laser at 532 nm generated using a frequency doubled Nd-YAG laser (Thales Laser SA, France, model: SAGA). A pulsed 450 W xenon arc lamp was used as the optical probe which is focused at the sample cell and directed perpendicular to the excitation pulse. The probe pulse is spectrally dispersed by a spectrograph and the time-resolved transient absorption spectra were recorded using an ICCD camera (Andor, UK, Model: iStar-320T). Temporal decay kinetics at selected wavelengths were recorded using a photomultiplier tube (Hamamatsu R920) connected to a 200 MHz digital oscilloscope.

Binding Kinetics Experiment

Binding kinetics of the sensitizers on TiO_2 surface was studied by recording the absorption spectra of dye solution at a regular time interval. First, the measured amount of dye was added into 40 ml of MeOH and then it was stirred to make a clear solution. 50 mg of TiO_2 was charged into the resulting solution and subsequently it was kept under stirring condition at room temperature in dark condition. Eventually, at a particular time interval, 3 ml of aliquot was collected, centrifuged at 3500 rpm and then the supernatant was taken to study the absorption spectra.

Results and Discussion

The stepwise synthesis protocols of the sensitizers have been depicted in Scheme 1. Sensitizers (**R1, R2** and **R3**) were synthesized using simple two step process. In order to improve the ligand solubility, hydrothermal treatment was undertaken in our synthesis methodology. Comparing with the other synthetic processes,[14] this method is exemplifying a simple route for synthesis of mononuclear ruthenium sensitizers. First **I1** ([Ru(H$_2$dcbpy)$_2$Cl$_2$] where H$_2$dcbpy is *2,2'-bipyridine-4,4'*-dicarboxylic acid) was synthesized hydrothermally using RuCl$_3$.xH$_2$O and *2,2'-bipyridine-4,4'*- dicarboxylic acid in presence of HCl (37 wt%) whereas, **I2** ([Ru(dnbpy)$_2$Cl$_2$] where dnbpy is *4,4'-Dinonyl-2,2'*-bipyridine) was synthesized by following the earlier reported non-hydrothermal method in presence of RuCl$_3$.xH$_2$O, *4,4'-Dinonyl-2,2'*-bipyridine and LiCl.[15] Finally, the Ru^{II} sensitizers were obtained from the hydrothermal reaction of **I1** and **I2** with the 8-hydroxyquinoline and its acid derivative as the ancillary chelating ligand. All three sensitizers were characterized using ^{1}H NMR, mass and FT-IR spectroscopy and elementary analysis (ESI†).
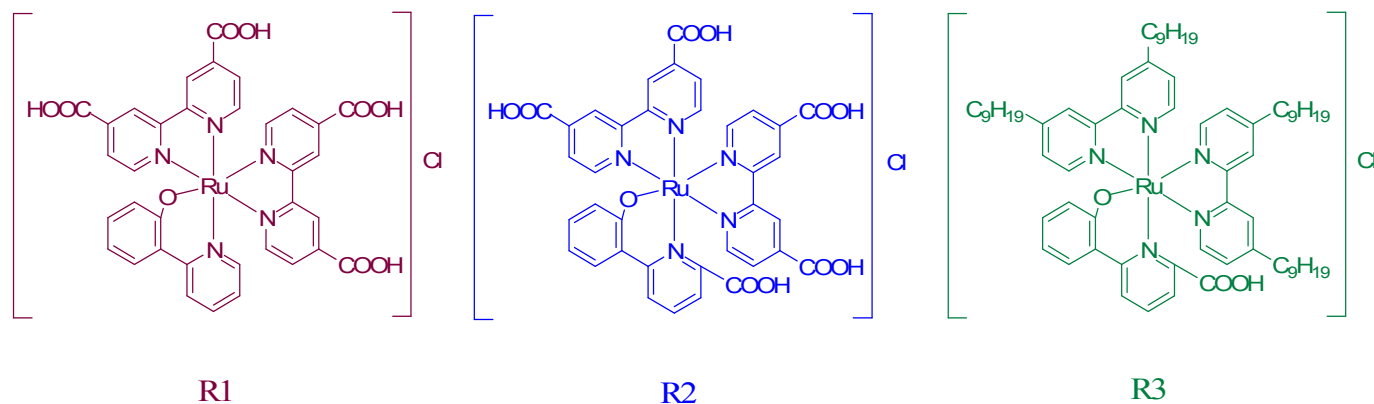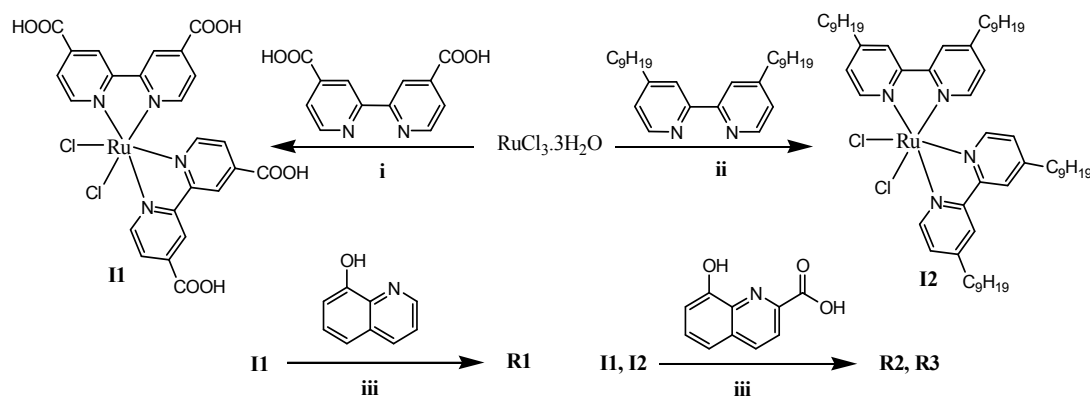
Fig. 1 Molecular structures of **R1**, **R2** and **R3** sensitizers.

Scheme 1. Stepwise synthesis of sensitizers. Reagents and conditions: (i) 1.5 ml H_2O, 1.5 ml HCl, 200 °C for 4 h;(ii) LiCl, DMF (50 ml), reflux for 8 h; (iii) 10 ml DMF, 170 °C for 5 h.

Absorption spectra of the sensitizers were recorded in methanolic solution at room temperature (Fig. 2a) and the pertinent information was appended in Table 1. **R1** and **R2** have a close spectral pattern, also reflects their structural similarities. These two sensitizers possess an absorption band at 470 nm and 472 nm, which attributes to MLCT transition. Red-shifted absorption maxima of **R2** may due to the presence of an additional electron withdrawing –COOH group in the HQ ligand.
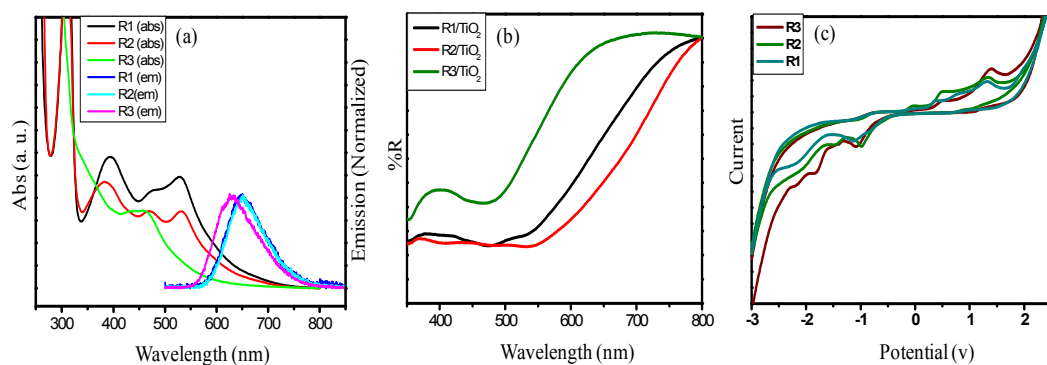
Fig. 2 (a) Absorption and emission spectra (normalized) of **R1**, **R2** and **R3** in methanol. (b) DRS of different Dye/TiO$_2$ composites. CV of different ruthenium sensitizers. Redox potentials were measured by cyclic voltammetry in MeOH with 0.1 M tetrabutylammonium hexafluorophosphate (TBAPF$_6$) as electrolyte, Ag/Ag$^+$ as reference electrode and with a scan rate of 100 mVs^{-1}.

The absorption maxima of the **R1** and **R2** complex are in higher wavelength region while compared to prototype [Ru(bpy)$_3$]$^{2+}$ complex. The HQ ligand is known to destabilize the ruthenium t$_{2g}$ orbitals due to strong sigma donating nature.[16a] Thus, the MLCT transition energy from the Ru(dπ) orbital to ligand (bpy or HQ) π* orbital is lowered, leading to lower energy absorption maxima in its UV-vis spectrum. Moreover, sensitizer **R2** showed lower molar extinction coefficient compared to **R1**. This may be attributed to the twisted nature of pyridine moiety of HQ ligand due to presence of an extra carboxylic group.[16b] **R3** displayed absorption maxima at around 458 nm, could be assigned as MLCT (dπ(Ru) $\rightarrow$ π*(ligand)) transition which is comparable to the spectral pattern of [Ru(bpy)$_3$]$^{+2}$.[17] The absorption maxima is in little higher energy in comparison to well known [Ru(bpy)$_3$]$^{+2}$, which may be due to destabilization of π* orbital of bipyridyl ligand having long chain alkyl group. Intense band in the UV region of all spectra assigned to the ligand centered π-π* transition. All the sensitizers have luminescent properties and exhibited emission maxima in the range of 628-652 nm, that we assigned to transition from ^{3}MLCT (dπ(Ru)) to π*(ligand) excited state. Furthermore, the energy gap between highest occupied molecular orbital (HOMO) and lowest unoccupied molecular orbital (LUMO) was also measured from the intercrossing point of the corresponding absorption-emission spectrum (Fig. 2a).

Table 1. Optical and electrochemical parameters of different sensitizers

Dye	$^a\lambda_{max}(\epsilon)M^{-1}cm^{-1}$[nm]	$^b\lambda_{max}$(Em.) (nm)	$^cE_{0-0}$ (eV)	^{d}PL lifetime (ns)	$^eE_{ox}$(V)	LUMO (V)
R1	529 (6100), 473 (5400)	648	2.06	417	0.4	-1.66
R2	532 (4275), 470 (4329)	652	2.22	395	0.5	-1.72
R3	458 (4300)	628	2.3	157	0.5	-1.8

^{a}Absorption and ^{b}emission spectra were recorded in MeOH solution at 298K. ^{c}The band gap, E$_{0-0}$, was derived from the intersection of the absorption and emission spectra. ^{d}Photoluminescence lifetime (emission) measured in MeOH solution at 298K. ^{e}Redox potentials were measured by cyclic voltammetry in MeOH with 0.1 M tetrabutylammonium hexafluorophosphate (TBAPF$_6$) as electrolyte, Ag/Ag$^+$ as reference electrode and with a scan rate of 100 mVs^{-1}.

To enquire the optical properties of metal complex sensitizers after being surface attached onto TiO$_2$, diffuse reflectance spectroscopy (DRS) was carried out for all Dye/TiO$_2$ composites, where the spectra have been recorded in the reflectance mode. As shown in Fig. 2b, optical properties of the Dye/TiO$_2$ composites complement the optical features of individual sensitizer. The extended long tail towards far-visible region (up to 800 nm) for all dyes is prominent in their corresponding Dye/TiO$_2$ composites. Lower energy absorption bands for **R1**, **R2** and **R3** are red-shifted and broadened after sensitizer being anchored on TiO$_2$ surface, which supports the formation of esteric linkage on TiO$_2$ surface. We observed a greater red shift for **R3** in DRS**,** which may due to less aggregation of **R3** in comparison to **R2** and **R1**. Similar phenomenon is also found to be common for N719 dye.[18] It is also worth mentioning that, all Dye/TiO$_2$ composites and TiO$_2$ shows characteristic absorption band around 380

nm due to its fundamental absorption of Ti–O bond in ultraviolet light range. The formation of esteric linkage between dye and TiO$_2$ was further supported by FT-IR analysis (Fig. S1†). The characteristic stretching frequency of C=O in –COOH moiety for **R1**, **R2** and **R3** appeared at 1721 cm^{-1}, 1725 cm^{-1} and 1772 cm^{-1} respectively. While comparing the FT-IR spectrum, it is clear that the intensity of C=O absorption peaks is weaker in dye adsorbed TiO$_2$ samples. This attributes to chemical adsorption of the dyes onto the TiO$_2$ particles via ester-like binding between the carboxylic acid groups and the OH moieties on TiO$_2$.[19]

For better understanding of excited state properties of the sensitizers, time resolved luminescence analysis was performed using CH$_3$OH as solvent. In solution state at 298 K, **R1** showed the maximum luminescence lifetime of 417 ns whereas that of **R3** is 157 ns (Fig. S2†, Table 1). The short-lived excited state of **R3** is likely due to efficient non-radiative decay via strong spin–orbit coupling. Even this excited-state lifetime (157 ns) of **R3** is still sufficient for electron injection into the conduction band (CB) of the TiO$_2$ electrode, because the injection from the ^{3}MLCT state to the TiO$_2$ CB occurs on a timescale of 10–100 ps.[20]

To investigate the electrochemical properties of the Ru^{II} sensitizers and to evaluate the possibility of electron injection from excited sensitizer to the CB of TiO$_2$, cyclic voltammetry (CV) was performed with 0.1 M tetrabutylammonium hexaflurophosphate as supporting elctrolyte in CH$_3$OH solution (Fig. 2c). Redox potential of the dyes have also been determined from their corresponding peak potential and incorporated in Table 1. The oxidation potential of the sensitizers are 0.4 V, 0.5 V and 0.5 V (*vs.* ferrecene, Fc/Fc$^+$) and the calculated LUMO energy values are -1.66, -1.72 and -1.8 V vs. NHE for **R1, R2** and **R3,** which indicates that the LUMO level is sufficiently negative for energetically favourable photo-induced excited state electron injection, while considering the CB alignment of the TiO$_2$.[21]

Dynamics of MLCT in the excited states of ruthenium polypyridyl complexes have shown promise for artificial solar energy harvesting.[22] To understand the catalytic efficiencies of the studied ruthenium complexes, we have compared the photophysical properties of three complexes using nanosecond flash photolysis experiments in methanol. Fig. 3a shows the nanosecond transient absorption spectra following excitation of the complexes at 532 nm. The spectra shows bleach signal in 400-500 nm region corresponding to the ground state absorption and the excited state absorption signal at 300-400 nm region.

In case of **R1** and **R2**, the ESA consist of two bands with maxima at 335 nm and 390 nm. Appearance of two bands suggests that the excited state is in equilibrium of two types of MLCT states, namely, bipyridyl localized MLCT and HQ localized MLCT states. In **R3**, the single ESA band with maximum at ~380 nm suggests that a single MLCT state is involved in the relaxed excited state as in **R3**, the bipyridyl ligand substituent are changed from electron withdrawing carboxylic acid to long chain alkyl groups. The result attributes to destabilization of the bipyridyl LUMO energy level. In consequence, the electronic structure of lowest energy state is dominated by HQ localized MLCT state. Different nature of electronic structures in excited triplet state of **R3** as compared to **R1** and **R2** are also apparent from the excited state lifetime, evaluated from their respective kinetic profile monitored at 390 nm (Figs. 3b and 3c). In aerated sample, the excited state lifetime of **R3** is lower with 160 ns as compared to the lifetime of **R1** (410 ns) and **R2** (370 ns). In deaerated solution, the lifetime of the excited state increases significantly due to

absence of non-radiative deactivation by oxygen quenching. However, the lifetime of **R3** remains shorter than that of **R1** and **R2**, due to different nature of electronic structure of the lowest excited state. Thus it is worth mentioning that, the excited state lifetimes of all the complexes are sufficiently long to inject electron from the MLCT state to the TiO$_2$ CB in sensitized sample, which is a critical step in deciding the catalytic activity of the sensitizers. Thus, the difference in hydrogen generation efficiencies cannot be fully correlated with the excited state lifetime of the complexes rather other factors must be playing dominant role.
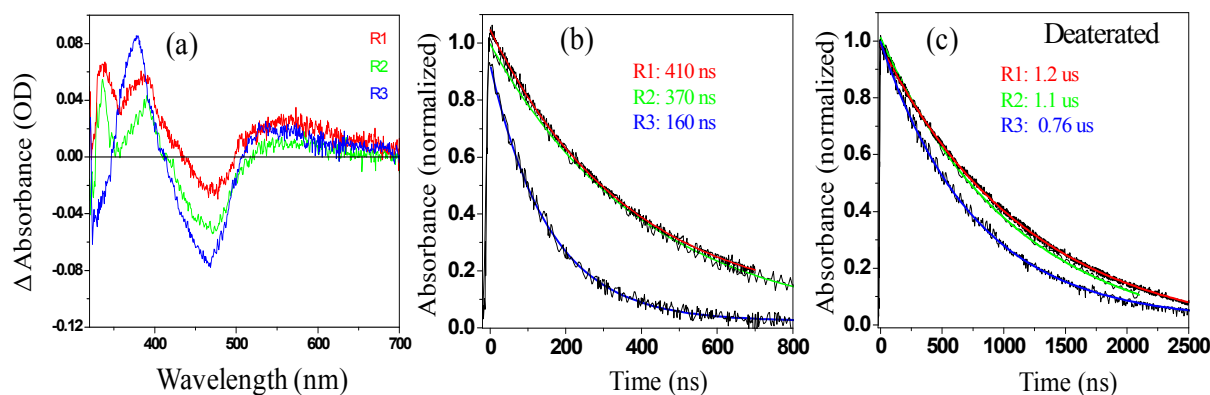

Fig. 3 (a) Time-resolved absorption spectra of different sensitizers at 5 ns following 532 nm laser excitation. The kinetic decay profiles of dyes **R1-R3** in methanol solution at (b) aerated and (c) deaerated condition. The kinetics was monitored at 390 nm.

Adsorption kinetics

We have investigated the adsorption kinetics of HQ coordinated Ru-sensitizers on TiO$_2$ surface using ~10^{-5} M dye solutions and 50 mg of TiO$_2$, and the results were depicted in Fig. 4. Typically, in photocatalytic hydrogen evolution reaction using dye adsorbed TiO$_2$, the amount of dye adsorbed on to TiO$_2$ surface is estimated spectrophotometrically by measuring the difference in absorbance of free dye in solution with that of the supernatant liquid obtained after filtration/centrifugation. Here, the amount of anchored dye (at equilibrium dye loading) on powder TiO$_2$ surface was measured as a function of suspension (adsorption) time. We can get a closer idea on the rate of adsorption of each dye onto TiO$_2$ surface by fitting the data on a first order exponential decay equation as mentioned below.

$$Abs(t) = Abs(eq) + Ae^{-(kt)}$$

Here, Abs(t) is the absorbance of the unabsorbed dye at particular time t, Abs(eq) is absorbance of the unabsorbed dye at equilibrium loading condition, A is fitting constant and k (min^{-1}) is rate constant for adsorption kinetics in terms of unabsorbed dye that remain in the solution. The greater k value signifies the slower rate of dye absorption and vice verse. As shown in Fig. 4, the calculated k values are in good accordance with the anchoring group present in dye molecule. The highest k value of 24.2 min^{-1} is attributable to the slow absorption of **R3** which has one anchoring group. Thus a very close hydrogen evolution activity of **R2** and **R3** may be attributed to the blocking of electron-hole recombination between titania and the oxidized SED species by

long aliphatic chain unit attached to bipyridine moieties in **R3**. The similar phenomena have been reported by Durant and co-workers in dye sensitized solar cell application.[23] The estimated equilibrium loading of the sensitizers for 10 mg of TiO_2 were 0.8 µmol, 0.6 µmol, 0.34 µmol for **R1**, **R2** and **R3** respectively. Indeed, it can be speculated that the additional carboxyl group in hydroxyquinoline moiety of **R2** does not have any role for participating in the binding to TiO_2 surface.[24] The kinetic competition results are also in good accordance with the low hydrogen evolution efficiency and high optimized dye loading of **R3**.
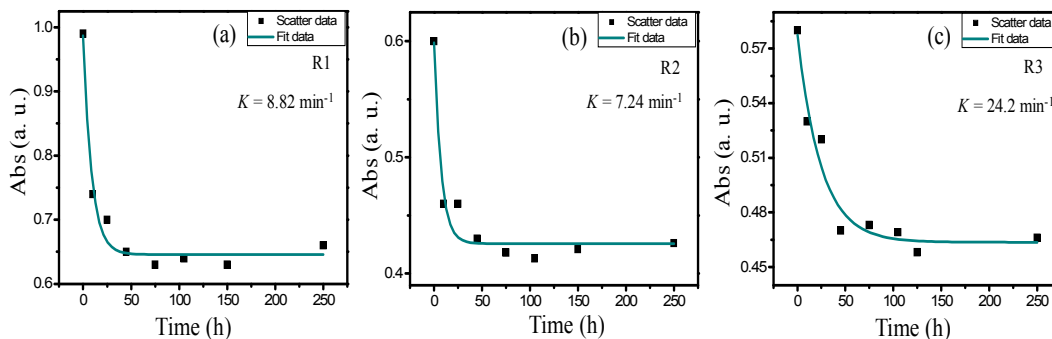

Fig. 4 Adsorption kinetics of different sensitizers at concentration ~ 10^{-5} M in presence of 50 mg TiO_2 at room temperature.

Photocatalytic hydrogen generation

To assess the performance of these dyes for photocatalytic proton reduction from water SED mixture, the photocatalytic experiment of Dye/Pt-TiO_2 systems (containing dyes **R1**, **R2**, and **R3**) was investigated in 20 ml of 10 vol% aqueous triethanolamine (TEOA). All Dye/Pt-TiO_2 catalysts were fabricated using commercially available TiO_2 anatase particles platinized by photo-deposition of Pt in methanol using a Xe lamp (450 W).[25] After this photo-deposition, the dye was adsorbed onto the Pt-TiO_2 particles by solution processing in the presence of dye solution in methanol at room temperature for 12 h. Scanning electron microscope (SEM) and transmission electron microscope (TEM) studies were carried out to observe the morphology of dye/Pt-TiO_2. TiO_2 particle are mostly uniform in size and unsymmetrical spherical in nature with particle size of ~25 nm (Fig. S3†).

The obvious effect of the sensitizers for photocatalytic H_2 production was shown in Fig. S4† as **R1** sensitized photocatalyst showed high H_2 production yield in comparison to bare and platinized TiO_2 under similar experimental condition. As shown in Fig. 5a and Table 2, **R1** exhibits the greater efficiency with H_2 generation yield 225 µmol (1734 TON), which is considerably higher than that of **R2** (137 µmol with 1056 TON) though **R2** has one more carboxylic anchoring group. As expected from the molecular structure, the rate of adsorption for **R2** is also slightly higher in comparison to **R1**. Indeed, the higher photoactivity of **R1** factually resembles higher emission lifetime of electron, as evidenced from their respective time resolved luminescent studies.

Table 2. Solar driven H_2 production over different Dye/ Pt-TiO$_2$

Dye	TON[a]	Amt. of H_2 (μmol)
R1	1734	225.2
R2	1056	137.2
R3	891	115.8

[a]Turn Over Number was calculated after 6 h using, TON = (2 x Amount of H_2)/ Amount of sensitizer}

In contrary, a very lower photoactivity was expected for **R3** which has only one anchoring group. But it showed a close H_2 production efficiency with **R2**. This result may due to the more negative energy of the LUMO level in **R3** which promotes easy electron transfer from dye to CB of TiO$_2$. Moreover, as-confirmed by the DRS analysis, long bulky chain effectively retarded the aggregation of **R3** on TiO$_2$ surface, which may also facilitate the effective electron injection from the dye molecule to TiO$_2$. Thus it is worth mentioning here that besides the energy of LUMO level, electron injection from dye to TiO$_2$ is also depends on the number carboxylic groups, its stereochemical position in the molecule which influences the dye absorption and formation of electron transfer path.[26]

To correlate the adsorption property of sensitizers and the H_2 production activity, we have also performed a sequential experiment with different amount of dye loaded Pt-TiO$_2$ (Fig. S5†). The optimized concentration for **R1, R2** and **R3** are 0.1μmol, 0.1 μmol and 0.25 μmol/10 mg of respective Pt-TiO$_2$ composites. High optimized loading for **R3** is due to the presence of one carboxyl group and greater equilibrium loading at TiO$_2$ surface. pH has a great influence on existing state of the dye, electron donor reagent and esteric bond that forms in between dye and TiO$_2$.[27] The effect of pH has been screened with all Dye/Pt-TiO$_2$ in aqueous TEOA medium where the pH was adjusted by addition of 1(M) HCl (Fig. 5b). The rate of H_2 production was decreased immensely at pH 4 for all photocatalysts. This is because in acidic medium protonation of the surface titanol groups inhibited the formation of, esteric linkage effectively.[3a] Whereas at neutral medium the photocatalysts are giving the maximum efficiency and immediately fall down when pH was maintained at 10. At higher pH, the carboxyl groups of sensitizers were deprotonated, so the dye could not adsorb on TiO$_2$ surface effectively because of electrostatic repulsion force. Moreover, TEOA was protonated in acidic solution, so its ability of donating electrons would weaken, which might influence the regeneration of oxidized dye molecules. It is well-known that in aqueous solutions, the band edges of TiO$_2$ display a Nernstian dependence with the solution pH, moving ~60 mV per pH unit due to surface protonation/deprotonation.[28] This could be a reason for change in the thermodynamic driving force for charge injection from dye to TiO$_2$ conduction band. In a dye-sensitized system, dye desorption under long term stirring under aqueous conditions is inevitable.[29] Finally, the effect of the different Pt loading was also tested to screen the hydrogen evolution activity. Fig. 5c shows temporal plots for the H_2 generation using the catalysts of 0.25 *μ*mol dye/10 mg Pt-TiO$_2$. The H_2 production rate increased with the Pt load until a maximum at 1 wt% and decreased with further noble metal loading.[30] Moreover the stability of the R1 sensitizer was examined over 24 h. The rate of H_2 evolution was reduced gradually

from 2nd catalytic cycle (Fig. S6†). The lowering of photoactivity may be due to partial dissolution of dye and consumption of
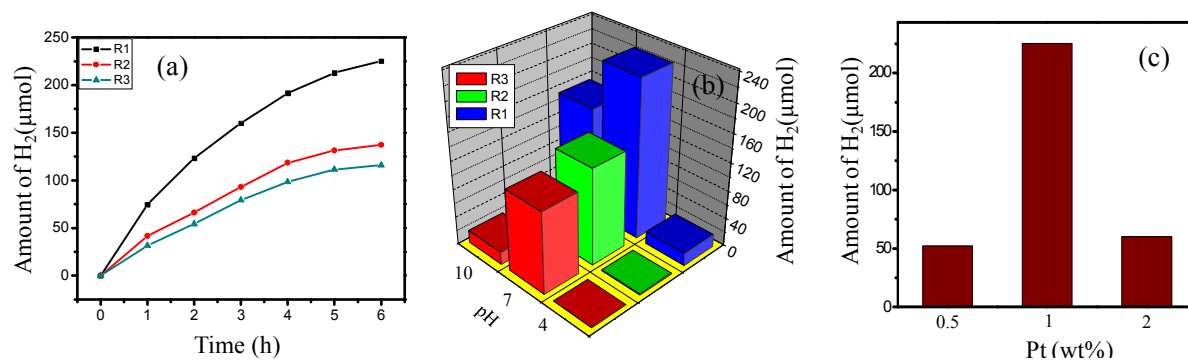
sacrificial electron donor.

Fig. 5 (a) Time courses of photocatalytic H$_2$ evolution over different Dye/Pt-TiO$_2$ composite (b) Amount of the H$_2$ production at different pH. (c) Effect of the Pt variation on H$_2$ evolution. Reaction condition: 10 of Dye/Pt-TiO$_2$ with optimized dye concentration, 20 ml of 10% v/v aqueous TEOA solution, Xe lamp set at 400 W which is equipped with 420 nm cut-off filter and room temperature.

To obtain a further insight into the electronic structure and molecular orbital structure of ground state, density functional theory

(DFT)[31] calculations were carried out using Materials Studio 6.1 software program package. Ground state geometry was fully

optimized using Forcite module. With optimized ground state geometry, single point calculation was performed to calculate the

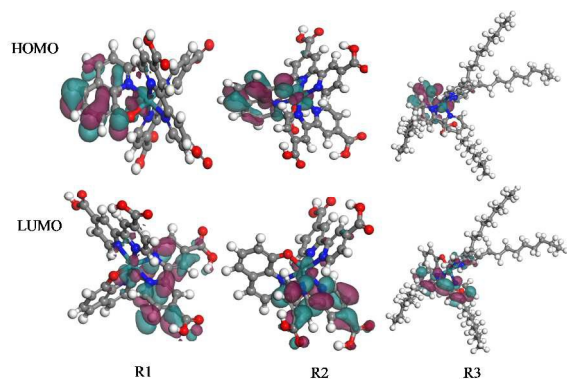molecular orbitals using DMol3 module at B3LYP/dnd functional.

Fig. 6 Isodensity surface for HOMO and LUMO molecular orbitals of **R1**, **R2** and **R3**.

As shown in Fig. 6, HOMO of the **R1, R2** and **R3** are mainly populated over the ruthenium metal and LUMO are predominantly

localized over polypyridyl. Moreover, HOMO orbital of sensitizers have predominant ruthenium t$_{2g}$ character. On the other hand,

the orbital contributions towards the LUMO of the as-prepared sensitizers are quite similar to each other because the LUMO

results mainly from the orbital delocalization of the polypyridyl moieties of the ancillary ligands. Upon photoexcitation, the electron density moved from Ru-O and/or Ru-N unit to the polypyridyl moiety.
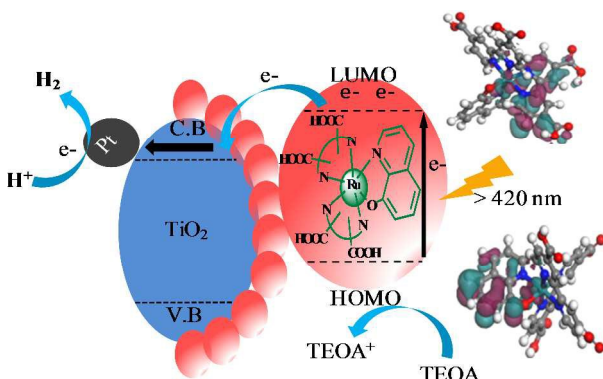

Fig. 7 Graphical representation of dye sensitized photocatalytic hydrogen production.

Based on the analytical/structural characterizations and photocatalytic experimental observations, the conceptual mechanism for photocatalytic hydrogen evolution has been diagrammatically represented in Fig. 7. During photo-excitation, the major electron density of HOMO (mainly delocalized on Ru-N and/or Ru-O units) moves to LUMO (majorly located on the ancillary ligand) of the dye, which undergoes a rapid vectorial transfer from LUMO to TiO_2 CB. It is indeed the esteric linkage between dye and TiO_2, which acts as the electron transfer path. Subsequently, electrons reduce the water molecules at the Pt centre. The as-prepared sensitizers possess long-lived ^{3}MLCT excited states, which provides sufficient time for electron injection from the ^{3}MLCT state to the TiO_2 conduction band. The regeneration of the oxidized dye species takes place in a consecutive manner when SED donates electron into the HOMO level of the oxidized dye species.

Conclusion

In conclusion, we have successfully demonstrated the electronic and structural properties of the newly synthesized ruthenium (II) sensitizers, featuring suitable photophysical properties to realize photocatalytic hydrogen evolution reaction over Pt-TiO_2 in aqueous triethanolamine medium. These cyclometalated ruthenium sensitizers exhibited broad optical absorptions of solar spectrum and long MLCT excited-state lifetime on nanosecond time scale. The sensitizer **R1** featuring underivatized hydroxyquinoline moiety and four carboxylic acid group appendage on bipyridyl moiety, exhibits the highest hydrogen production efficiency with TON 1734 after 6 h. We have also demonstrated that adsorption kinetics of sensitizers is an important parameter to be considered besides photophysical and electrochemical features, in order to achieve efficient hydrogen evolution activity. Introduction of the carboxyl group at hydroxyquinoline moiety resulted in increased rate of dye adsorption and decreased equilibrium loading on TiO_2 surface in comparison to **R1**. In case of **R3**, we have found efficient retardation of

electron-hole recombination between titania and the oxidized SED species by recombination-blocking effect of the attached bulky 4,4'-dinonyl unit in the ancillary, however it decelerated the kinetics of dye binding on TiO_2 surface. The calculated LUMO energy values and lifetime of electrons in the excited state ensures the favorable electron injection from dye to TiO_2 nanoparticles. In sharp contrast, the hydrogen evolution activity follows the order **R1**>**R2**>**R3** under similar experimental condition. These encouraging finding insist us to synthesize more derivatives of hydroxyquinoline based ruthenium complexes in order to tune their physical characteristics to improve photocatalytic activity towards solar hydrogen production.

Acknowledgements

Notes and references

1. A. Fujishima and K. Honda, *Nature,* 1972, **238**, 37-38.

2. B. O'Regan and M. Grätzel, *Nature,* 1991, **353**, 737-740.

3. (a) S. Ardo and G. J. Meyer, *Chem. Soc. Rev.*, 2009, **38**, 115-164; (b) F. Bella, C. Gerbaldi, C. Barolob and M. Grätzel, *Chem. Soc. Rev.* 2015, **44,** 3431-3473; (c) M. Watanabe, H. Hagiwara, A. Iribe, Y, Ogata, K, Shiomi, A, Staykov, S, Ida, K,Tanaka and T. Ishihara, *J. Mater. Chem. A*, 2014, **2**, 12952-12961; (d) D. Chatterjee, *Catal. Commun.*, 2010, **11**, 336–339; (e) D. Chatterjee, S. K. Moulik, L. Giribabu and R. K. Kanaparthi, *Transition Met. Chem.*, 2014, **39**, 641-646.

4. (a) J. H. Yum, E. Baranoff, S. Wenger, Md. K. Nazeeruddin and M. Gratzel, *Energy Environ. Sci.,* 2011, **4,** 842-857; (b) T. Kinoshita, J. T. Dy, S. Uchida, T. Kubo and H. Segawa, *Nat. Photonics,* 2013, **7**, 535-539. (c) V. K. Singh, R. K. Kanaparthi and L. Giribabu, *RSC Adv.*, 2014, **4**, 6970–6984.

5. C-C. Chou, K-L. Wu, Y. Chi, W-P. Hu, S. J. Yu, G-H. Lee, C-L. Lin and P-T. Chou, *Angew. Chem. Int. Ed.*, 2011, **50,** 2054-2058.

6. A. Listorti, B. O'Regan and J. R. Durrant, *Chem. Mater.*, 2011, **23,** 3381-3399.

7. T. Swetha, I. Mondal, K. Bhanuprakash, U. Pal and S. P. Singh, *ACS Appl. Mater. Interfaces*, **2015**, **7,** 19635-19642; (b) H-J. Park, W. Kim, W. Choi and Y. K. Chung, *New J. Chem.*, 2013, **37**, 3174-3182.

8. P. Jarosz, P. Du, J. Schneider, S.-H. Lee, D. McCamant and R. Eisenberg, *Inorg. Chem.,* 2009, **48,** 9653-9663.

9. S. Bala, I. Mondal, A. Goswami, U. Pal and R. Mondal, *Dalton Trans.*, 2014, **43,** 15704-15707.

10. (a) X. Zhang, B. Peng, T. Peng, L. Yu, R. Li and J. Zhang, *J. Power Sources,* 2015, **1,** 30-37; (b) W. Kim, T. Tachikawa, T. Majima, C. Li, H-J. Kim and W. Choi, *Energy Environ. Sci.,* 2010, **3,** 1789-1795.

11. K. Takanabe, K. Kamata, X. Wang, M. Antonietti, J. Kubota and K. Domen, *Phys. Chem. Chem. Phys.,* 2010, **12,** 13020-13025.

12. X. Zhang, U. Veikko, J. Mao, P. Cai, T. Peng, *Chem. Eur. J.*, 2012, **18,** 12103-12111.

13. E. Eskelinen, S. Luukkanen, M. Haukka, M. Ahlgrén and T. A. Pakkanen, *J. Chem. Soc.*, *Dalton Trans*., 2000, 2745-2752.

14. Md. K. Nazeeruddin, C. Klein, P. Liska and M. Grätzel, *Coord. Chem. Rev.,* 2005, **249**, 1460-1467.

15. B. P. Sullivan, D. J. Salmon and T. J. Meyer, *Inorg. Chem.* 1978, **17,** 3334-3341.

16. (a) R. B. Sears, L. E. Joyce and C. Turro, *Photochem. Photobiol*., 2010, **86,** 1230-1236. (b) X. Qian, Y-Z. Zhu, J. Song, X-P. Gao and J-Y. Zheng, *Org. Lett.* 2013, **15,** 6034-6037.

17. P. Müller and K. Brettel, *Photochem. Photobiol. Sci.,* 2012, **11**, 632-636.

18. L. Wei, Y. Na, Y. Yang, R. Fan, P. Wang and L. Li, *Phys. Chem. Chem. Phys.,* 2015, **17,** 1273-1280.

19. C-Y. Cai, S-K Tseng, M. Kuo1, K-Y. A. Lin, H. Yang, R. H. Lee**,** *RSC Adv.*, 2015, **5**, 102803-102810.

20. S. E. Koops, B. C. O'Regan, P. R. F. Barnes and J. R. Durrant, *J. Am. Chem. Soc.*, 2009, **131,** 4808-4818.

21. D. O. Scalon, C. W. Dunnill, J. Buckeridge, S. A. Shevlin, A. J. Logsdail, S. M. Woodley, C. R. A. Catlow, M. J. Powell, R. G. Palgrave, I. P. Perkin, G. W. Watson, T. W. Keal, P. Sherwood, A. Walsh and A. A. Sokol, *Nat. Mater.* 2013, **12,** 798-801.

22. (a) T. Banerjee, A. K. Biswas, U. Reddy G, T. S. Sahu, A. Das, B. Ganguly, and H. N. Ghosh**,** *J. Phys. Chem. C*., 2014, **118**, 3864 – 3877; (b) R. Ghosh and D. K. Palit, *Phys. Chem. Chem. Phys*., 2014, **16,** 219-226.

23. J. E. Kroeze, N. Hirata, S. Koops, M. K. Nazeeruddin, L. Schmidt- Mende, M. Grätzel and J. R. Durrant, *J. Am. Chem. Soc.,* 2006, **128,** 16376-16383.

24. H. Ozawa, T. Sugiura, R. Shimizu, and H. Arakawa, *Inorg. Chem*., 2014, **53**, 9375−9384.

25. J. M. Herrmann, J. Disdier and P. Pichat, *J. Phys. Chem.,* 1986, **90,** 6028-6034.

26. (a) A. Hagfeldt and M. Gratzel, *Chem. Rev.,* 1995, **95,** 49-68; (b) T. Kajiwara, K. Hashimoto, T. Kawai and T. Sakata, *J. Phys. Chem.* 1982, **86,** 4516-4522; (c) T. Y. Peng, D. N. Ke, P. Cai, K. Dai, L. Ma and L. Zan, *J. Power Sources* 2008, **180,** 498-505; (d) T. Y. Peng, K. Dai, H. B. Yi, D. N. Ke, P. Cai and L. Zan, *Chem. Phys. Lett.* 2008, **460,** 216-219.

27. (a) Q. Li, L. Chen and G. Lu, *J. Phys. Chem. C,* 2007, **111,** 11494-11499; (b) U. Pal, S. Ghosh and D. Chatterjee, *Transition Met. Chem*., 2012, **37**, 93-96.

28. L. A. Lyon and J. T. Hupp, *J. Phys. Chem. B,* 1999, **103,** 4623-4628.

29. Q. Li, Z. Jin, Z. Peng, Y. Li, S. Li and G. Lu, *J. Phys. Chem. C,* 2007, **111,** 8237-8241.

30. X. Yu, A. Shavel, X. An, Z. Luo, M. Ibáñez and A. Cabot, *J. Am. Chem. Soc.,* 2014, **136,** 9236–9239.

31. P. Qin, X. Yang, R. Chen, L. Sun, T. Marinado, T. Edvinsson, G. Boschloo and A. Hagfeldt, *J. Phys. Chem. C,* 2007, **111,** 1853.

Throwing light on hydroxyquinoline-based ruthenium sensitizers with long-lived charge carrier boosts photocatalytic H$_2$ evolution

Indranil Mondal,[a,b] Amritanjali Tiwari,[a,b] Rajib Ghosh,[c] Ujjwal Pal [a,b] *

[a]Central Mechanical Engineering Research Institute, M. G. Avenue, Durgapur-713209, WB, India.

[b]Network of Institutes for Solar Energy (CSIR-NISE) and Academy of Scientific and Innovative Research (AcSIR)

[c]Radiation & Photochemistry Division Bhabha Atomic Research centre, Mumbai-400085, India